Article

Not peer-reviewed version

Cold-Pressed Insulation Boards from Recycled Cotton Fibers Using a Water-Borne PVAc-Starch Binder: Processing, Structure and Properties

Tadeáš Zachara *, Přemysl Šedivka, Vlastimil Borůvka, Kryštof Kubista, Tomáš Holeček, Martin Lexa, Lukáš Sahula, Adam Sikora

Posted Date: 11 February 2026

doi: 10.20944/preprints202602.0834.v1

Keywords: fiber-based composites; recycled cotton fibers, cold pressing; water-borne binder; thermal parameters; moisture-related behavior; mechanical properties

 doi:10.20944/preprints202602.0834.v1

Article

Cold-Pressed Insulation Boards from Recycled Cotton Fibers Using a Water-Borne PVAc-Starch Binder: Processing, Structure and Properties

Tadeáš Zachara *, Přemysl Šedivka, Vlastimil Borůvka, Kryštof Kubista, Tomáš Holeček, Martin Lexa, Lukáš Sahula and Adam Sikora

Faculty of Forestry and Wood Sciences, Czech University of Life Sciences Prague, Kamýcká 129, 16500 Prague, Czech Republic

* Correspondence: zachara@fld.czu.cz; Tel.: +420 773 112 779

Abstract

This study investigates the valorization of post-consumer and post-industrial recycled cotton fibers from textile waste into porous fiber-based insulation composites using a lowenergy cold-pressing process and a water-borne hybrid binder based on polyvinyl acetate (PVAc) and modified cornstarch. Insulation boards were produced with target densities ranging from 300 to 340 kg·m^{-3}, achieved by systematically adjusting the percentage weight fractions of recycled cotton fibers and binder components. The influence of board density on microstructure, inter-fiber bonding, and structure-property relationships was evaluated. The resulting boards exhibited thermal conductivity values between 0.0710 and 0.0739 W·m^{-1}·K^{-1}. Compressive strength measured at 10% relative deformation of the specimen thickness ranged from 46 to 162 kPa, while internal bond strength varied between 2 and 6 kPa. Water absorption decreased by approximately 18% with increasing density, indicating improved binder distribution and reduced open porosity. The PVAc–starch binder system enabled effective inter-fiber bonding without formaldehyde-based resins or energy-intensive curing, supporting a low-energy and circular processing concept for textile waste valorization. Overall, the results demonstrate that recycled cotton fibers represent a viable feedstock for porous insulation composites combining balanced thermal, mechanical, and moisture-related performance with reduced environmental impact.

Keywords: fiber-based composites; recycled cotton fibers; cold pressing; water-borne binder; thermal parameters; moisture-related behavior; mechanical properties

1. Introduction

The built environment is responsible for approximately 37% of global annual CO_2 emissions, with more than half of this originating from heat losses due to inadequately insulated building envelopes [1].

From a materials design perspective, new sustainable materials should combine low thermal conductivity, mechanical integrity, and low-toxicity chemistry. In 2025, European Union legislation mandates the separate collection and recycling of textile waste under Directive 2008/98/EC, as amended by Directive 2018/851/EC. This regulatory framework demands the development of new functional materials for the cascading use of textile fibers into sustainable products with added value, for example new thermal insulation materials. Recycled lignocellulosic or textile fibers contribute to the circular economy by diverting post-consumer waste from landfills, while requiring minimal additional energy for processing [2].

Among such resources, post-consumer cotton exhibits an intrinsic solid-phase thermal conductivity of approximately 0.04 W·m^{-1}·K^{-1} [3]. The primary challenge lies in transforming these

 doi:10.20944/preprints202602.0834.v1

hydrophilic, crimped fibers into cohesive, self-supporting boards without relying on formaldehyde-based or highly cross-linked synthetic resins.

Recent epoxy/flax-hemp laminates filled with waste glass dust achieved an effective thermal conductivity λ of approximately 0.30 $W \cdot m^{-1} \cdot K^{-1}$, but required a virgin epoxy matrix and curing at 120 °C [4]. Cellulose nanofiber aerogels crosslinked with melamine-urea-formaldehyde exhibited a λ of less than 0.025 $W \cdot m^{-1} \cdot K^{-1}$, though they were brittle and released free formaldehyde [5]. Cotton filter waste mats, hot-pressed with thermoplastic corn starch, reduced λ to 0.046 $W \cdot m^{-1} \cdot K^{-1}$, but their compressive strength remained under 20 kPa [6]. Epoxy syntactic foams containing hollow glass microspheres demonstrated hydrostatic pressure resistance and a λ of approximately 0.10 $W \cdot m^{-1} \cdot K^{-1}$, although at densities exceeding 500 $kg \cdot m^{-3}$ [7]. Hollow glass bead-filled carbon fiber/PEEK composites reduced λ by 45%, but their high cost and embodied energy limit their adoption in construction [8]. Nanocellulose-modified polyurethane foams exhibit a refined microstructure and a lower λ, yet they still rely on petrochemical-based materials [9]. A recent review highlights the rapid progress in natural fiber composite boards and bio-based adhesives, while also emphasizing the scarcity of panels that are both structurally sound and have low conductivity [10].

At the same time, regulatory and market signals are driving materials toward carbon transparency and circularity. The European Union's 2024 recast of the Energy Performance of Buildings Directive (EPBD) introduces phased requirements for whole-life carbon assessment and disclosure for new buildings, furthering the demand for low-impact insulation products [11]. Comparative life-cycle assessments (LCAs) indicate that plant-fiber and recycled-fiber materials can achieve lower cradle-to-grave impacts than mineral wool or petrochemical foams, particularly when functional performance is normalized and both biogenic carbon storage and end-of-life are properly accounted for [12]. These findings reinforce the rationale for utilizing recycled textile feedstocks, which not only diverts waste but also reduces processing energy.

From a materials and structural perspective, heat transfer in porous fiber-binder boards is governed by the solid fiber/polymer skeleton, gaseous conduction across the pore spectrum, and a radiative term that increases with cell size [13–16]. Thus, binder chemistry, volume fraction, and spatial distribution co-tune λ through interfacial contact resistance and the pore-size distribution established during consolidation [17–19]. For cellulosic (cotton) fibers, water-based PVAc offers low-toxicity processing and room-temperature film formation. However, moisture absorption can plasticize PVAc and weaken fiber-matrix load transfer on hydroxylated surfaces unless carefully controlled in the formulation [20–22]. In contrast, starch binders can be mildly cross-linked to enhance cohesive strength and reduce water uptake [23,24]. PVAc-starch hybrids thus improve wet resistance and interfacial adhesion while maintaining a water-based processing window [25,26].

In this work, a PVAc-starch hybrid binder is employed to enhance mechanical properties, maintain a fine pore structure that limits gaseous and radiative heat transfer, and reduce moisture-induced softening through mild cross-linking, enabling the design of bio-based fiber composites based on recycled cotton fibers for building insulation applications.

2. Materials and Methods

2.1. Recycled Cotton Fibers

The basic material used in this study was recycled cotton fibers EN-TEX (Enroll CZ, Nová Ves, Czech Republic), originating from mechanically processed post-consumer and post-industrial textile waste. Shredding and fiberizing refer to a purely mechanical size-reduction procedure in which textile residues are progressively torn, cut, and disintegrated into individual fibers, without inducing any chemical modification or thermal exposure. To establish the baseline characteristics of the recycled cotton feedstock, the fibers were analyzed in terms of their dimensions, morphology, and chemical composition. The size distribution analysis revealed a broad variability in both diameter and length. Fiber diameters mostly ranged between 8 and 15 μm, while fiber lengths were typically 400–900 μm. This heterogeneity reflects the random breakage of fibers during recycling.

 doi:10.20944/preprints202602.0834.v1

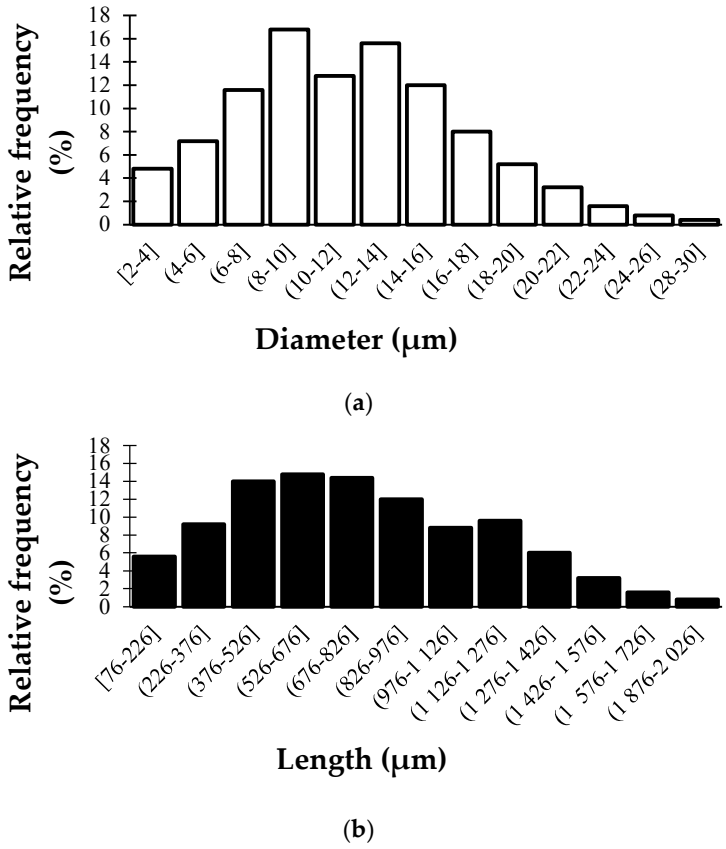

Figure 1. Histograms of fiber diameter (**a**) and fiber length (**b**) for recycled cotton feedstock.

In addition to the recycled fibers, the material contains integrated flame retardants based on aluminium hydroxide ($Al(OH)_3$) (ATH) in weight ration 2–3 % weight, applied in the form of a fine powder to the surface of recycled cotton fibers, ensuring classification in reaction-to-fire class E according to the European Technical Assessment ETA-19/0457 [27]. Further additives include antifungal agents compounds Sodium Bicarbonate (NaHCO3) in weight ration 1–2 % weight, and Zinc Pyrithione (C10H8N2O2S2Zn) in weight ration 1–2 % weight, that resist pests and rodents, which are commonly found in commercial cellulose-fiber-based insulation products. Both applied in the form of a fine powder to the surface of recycled cotton fibers; The fibers are supplied without synthetic binders or formaldehyde.

2.2. Binder Systems

One of the adhesives used in the composite production was a polyvinyl acetate PVAc-based water dispersion PROFIBOND (Profil Print Technology s.r.o., Všemyslice, Czech Republic). It is a one-component adhesive supplied as a white liquid dispersion with a density of 1.08 ± 0.01 g·cm^{-3}, a solids content of 50 ± 1%, a viscosity of 9500 ± 1500 mPa·s, and a pH of 4.75 ± 0.25. The adhesive provides water resistance corresponding to class D3 and does not contain formaldehyde.

Another adhesive used in the production of the composite boards was corn starch (Herold, Rakovník, Czech Republic), supplied as a fine white powder. The starch used in this study is a polysaccharide composed primarily of amylopectin (≈approximately 72–75%) and amylose (≈approximately 25–28%). Its granules are typically 5–25 μm in diameter, with a bulk density of 0.5–0.6 g·cm^{-3}, and a moisture content of less than 13%. The gelatinization temperature is approximately 62–72 °C, at which point the starch swells in water and forms a viscous gel.

 doi:10.20944/preprints202602.0834.v1

2.3. Microstructural Characterization

Recycled cotton fibers were characterized to establish their baseline morphology and chemistry prior to board fabrication. Their heterogeneous origin from post-consumer and post-industrial waste necessitated an evaluation of potential synthetic residues and inorganic additives, which may impact binder compatibility and composite performance. Morphology was examined using a scanning electron microscope MIRA3 (Tescan Orsay Holding, Brno, Czech Republic) equipped with an energy-dispersive spectroscopy Xplore 15 (Oxford Instruments plc, High Wycombe, Great Britain) system. Images were acquired at 200×, 1000×, 2000×, and 10,000× magnification and analyzed in ImageJ (ImageJ 1.53f, National Institutes of Health, Bethesda, MD, USA), with a total of 250 fibers measured after scale calibration. Elemental composition was determined using the ZAF quantification method. The chemical structure was assessed using FTIR (Nicolet iS20, Waltham, MA, USA; spectra collected in the range of 4000–600 cm^{-1}) to identify cellulose functional groups and possible chemical modifications, and Raman spectroscopy WITec alpha 300 (WITec Wissenschaftliche Instrumente und Technologie GmbH, Ulm, Germany) to evaluate cellulose crystallinity and detect synthetic residues.

2.4. Preparation of Thermal Insulation Boards

The boards were prepared with target densities of 300-340 $kg \cdot m^{-3}$, the range was set due to a balance between thermal resistance and mechanical integrity in fiber-based materials [28–30]. The density of the material depends on the weight fraction of the components cotton fibers, PVAc and cornstarch. Different weight ratios of the three components affect the properties of the composite. After weighing the required proportions of components, the given ratio of PVAc and cornstarch was applied while constantly stirring with a mechanical stirrer LGB (Imalpal S.r.l., San Damaso, Italy) at the constant temperature (20 ± 2 °C) and humidity (65 ± 5 %) environment. Test specimens with dimensions of 500 (L) × 300 (W) × 80 (T) mm were produced from the homogenized fiber-binder mixture, placed into molds, and pressed in a universal testing machine TT 2850 (TIRA, GmbH, Schalkau, Germany). The molds were lined with standardized support plates to ensure uniform pressure transfer during the process, and the same support configuration was used for all specimens, regardless of their target density or the specific PVAc-to-starch binder ratio applied in each formulation. The pressing of the mixture of gelatinized starch (65-70 °C) and PVAc adhesive occurred in a cold press, with the entire process completed in a single 2-minute cycle. The applied force varied with target density, ranging from 7.5 kN for the lowest-density boards (300 $kg \cdot m^{-3}$) to 25 kN for the highest-density boards (340 $kg \cdot m^{-3}$). The specimens were kept under load for approximately 1 hour, then technologically dried in drying chamber Binder FDL (Binder GmbH, Tuttlingen, Germany) and then air-conditioned in a climate chamber Memmert HPP 750 (Memmert GmbH, Schwabach, Germany) at a temperature of 20 ± 2 °C and a relative humidity of 65 ± 5 % for 14 days to reach an equilibrium moisture content.

The complete formulations and pressing parameters are summarized in Table 1.

Table 1. Composition of Test Specimens with Different Densities and Adhesives Ratio.

Density ($kg \cdot m^{-3}$)	Cotton fibers (%) *	PVAc (%) *	Corn starch (%) *	Pressing force (kN)
300	80	10	10	7.5
310	78	12	10	12
320	75	15	10	16
330	72	18	10	20
340	70	20	10	25

* Weight percent.

 doi:10.20944/preprints202602.0834.v1

2.5. Bulk Density Determination of Insulation Boards

The bulk density of the insulation boards was determined after conditioning at 20 ± 2 °C and 65 ± 5% relative humidity. Density was calculated as the ratio of the specimen mass to its geometrical volume. The mass of each specimen was measured using a laboratory balance, while the length, width, and thickness were determined using a digital caliper.

The bulk density ρ (kg·m^{-3}) was calculated according to Equation (1):

$$\rho = \frac{m}{V} \quad (1)$$

where m is the mass of the conditioned specimen (kg) and V is the specimen volume (m^3), calculated from the measured length, width, and thickness.

2.6. Thermal Parameters Characterization

Thermal conductivity λ and the thermal diffusivity a were measured using a thermal conductivity device ISOMET 2114 (Applied Precision Ltd., Bratislava, Slovakia) equipped with a needle probe sensor, in accordance with EN ISO 8301 [31]. Measurements were carried out on conditioned specimens under laboratory conditions (20 ± 2 °C, 65 ± 5% relative humidity). Based on the measured values, the volumetric heat capacity $\rho \cdot c$ and thermal diffusivity a were calculated according to Equation (2). For each density level, three independent board specimens were prepared, and thermal conductivity was measured at three different points on each specimen, resulting in nine measurements per variant. The reported values are presented as mean ± standard deviation. The thermal parameters were calculated using the following relationship:

$$a = \frac{\lambda}{\rho \cdot c} \quad (2)$$

where λ is the thermal conductivity (W·m^{-1}·K^{-1}), $c$is the specific heat capacity (J·kg^{-1}·K^{-1}), ρ is the bulk density (kg·m^{-3}), $\rho \cdot c$ is the volumetric heat capacity (J·m^{-3}·K^{-1}), and a is the thermal diffusivity (m^2·s^{-1}).

2.7. Moisture-Related Behavior Characterization

Moisture-related behavior of the boards was evaluated in accordance with EN ISO 29767 [32]. Specimens with dimensions of 200 mm (L) × 200 mm (W) × 80 mm (T) were prepared from conditioned boards. Water absorption and thickness swelling were determined by specimens weighed in the conditioned state and reweighed after 24 hours of immersion in tap water at a temperature of 20 ± 2 °C. After immersion, excess surface water was removed, and dimensional changes were recorded simultaneously. Measurements were performed under laboratory conditions (20 ± 2 °C, 65 ± 5% relative air humidity). For each density level, five specimens were tested, and the results are reported as mean ± standard deviation. Water absorption (WA) and thickness swelling (TS) were calculated using the following relations:

$$WA(\%) = \frac{m_2 - m_1}{m_1} \times 100 \quad (3)$$

$$TS(\%) = \frac{t_2 - t_1}{t_1} \times 100 \quad (4)$$

where m_1 is the specimen mass after conditioning (g), m_2 is the specimen mass after immersion (g), t_1 is the initial specimen thickness (mm), and t_2 is the thickness after immersion (mm).

2.8. Mechanical Properties Characterization

Compressive behavior of the thermal insulation boards was determined in accordance with EN ISO 29469 [33] using a universal testing machine TT 2850 (TIRA GmbH, Schalkau, Germany) (Figure 2a). Stress-strain curves were recorded up to 10% relative deformation of the specimen thickness. The

 doi:10.20944/preprints202602.0834.v1

load was applied continuously at a crosshead speed corresponding to a strain rate of 10 % min^{-1} (≈8 $mm \cdot min^{-1}$ for 80 mm thick samples). For each density level, ten conditioned specimens with dimensions of 50 mm (L) × 50 mm (W) × 80 mm (T) were tested, and the results are reported as mean ± standard deviation. Compressive strength (σ_{10}) was calculated as follows:

$$\sigma_{10} = \frac{F}{A} \tag{5}$$

where σ_{10} is the compressive stress at 10 % deformation (Pa), F is the applied load at 10% deformation (N), and A is the loaded cross-sectional area of the specimen (m^2).

For the assessment of board cohesion and resistance to tensile loading perpendicular to the board plane, internal bond strength was determined in accordance with EN ISO 29766 [34] using a universal testing machine TT 2850 (TIRA GmbH, Schalkau, Germany) (Figure 2b). Specimens with dimensions of 50 mm (L) × 50 mm (W) × 80 mm (T) were prepared in the conditioned state. The load was applied continuously at a rate of 2 $mm \cdot min^{-1}$ until failure. For each density level, ten specimens were tested, and the results are reported as mean ± standard deviation. Internal bond strength was calculated as follows:

$$\sigma_{ib} = \frac{F}{A} \tag{6}$$

where σ_{ib} is the internal bond strength (Pa), F is the maximum load at failure (N), and A is the loaded cross-sectional area of the specimen (m^2).

The experimental data obtained in this study were processed and evaluated using a combination of graphical and tabular methods. Statistical analyses were performed using STATISTICA (TIBCO Software Inc., Palo Alto, CA, USA), while selected graphs were prepared in Microsoft Excel (Microsoft, Redmond, USA). Basic descriptive statistics were applied to summarize the measured thermal, mechanical, and moisture-related properties of the insulation boards.

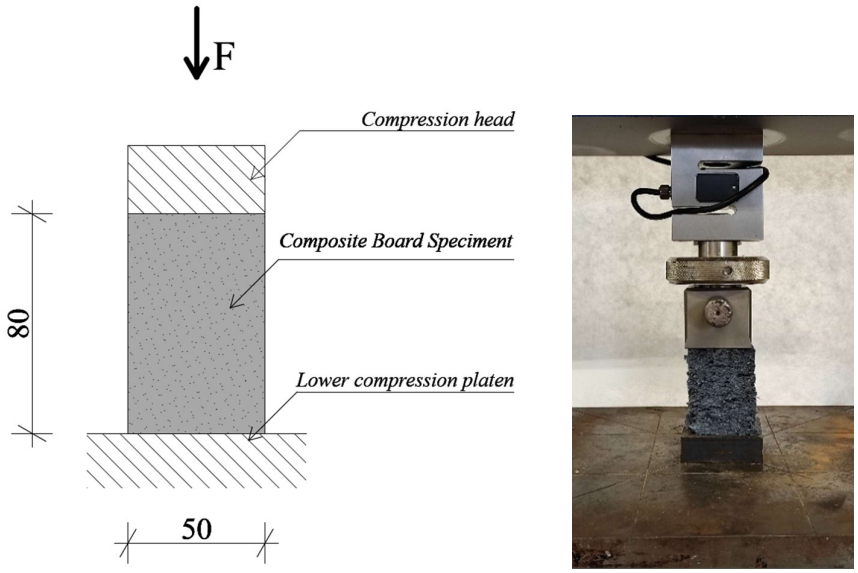

(**a**)

 doi:10.20944/preprints202602.0834.v1

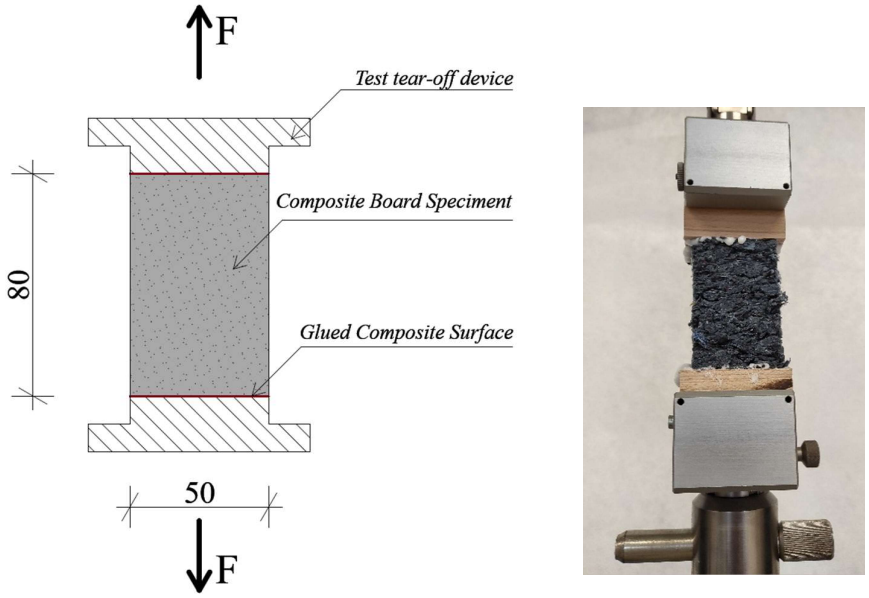

(**b**)

Figure 2. Schematics of the mechanical testing setups: (**a**) compression test configuration according to EN ISO 29469 [33], and (**b**) tensile strength test perpendicular to the board plane according to EN ISO 29766 [34].

3. Results and Discussion

3.1. Fiber Morphology and Chemical Composition

SEM analysis confirmed the heterogeneous morphology of recycled cotton fibers. At low magnification, the fibers formed an entangled network with numerous broken ends resulting from mechanical tearing (Figure 3a). Higher magnifications revealed twisted shapes, roughness, and longitudinal cracks (Figure 3b,c), while the highest magnification showed fine cracks and adhering particles (Figure 3d). These features enlarge the surface area for binder adhesion but simultaneously indicate reduced intrinsic fiber strength.

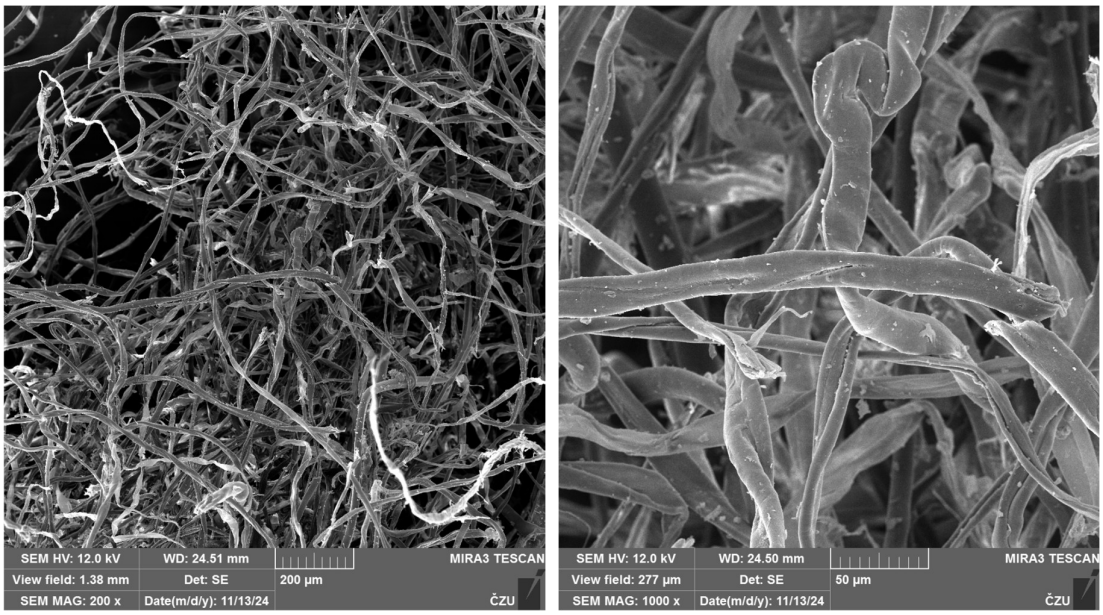

(**a**) (**b**)

 doi:10.20944/preprints202602.0834.v1

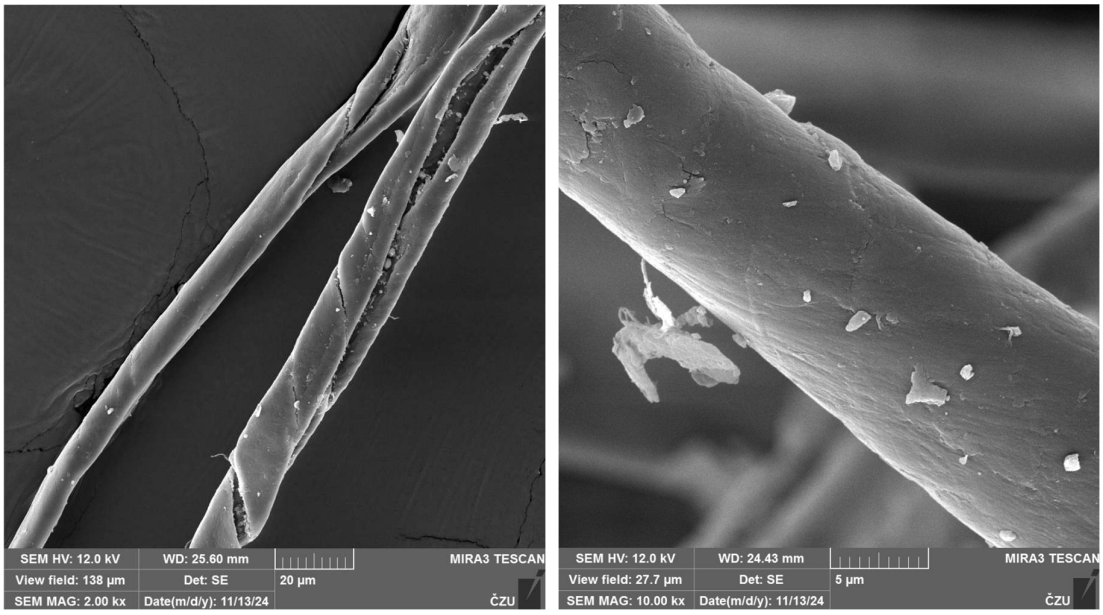

(**c**) (**d**)

Figure 3. SEM images of recycled cotton fibers at magnifications of (**a**) 200×, (**b**) 1000×, (**c**) 2000×, and (**d**) 10,000×.

The observed heterogeneity in fiber dimensions reflects the random breakage caused by mechanical recycling and is consistent with previous reports on mechanically recycled cotton [35]. This variability in aspect ratio plays a dual role in composite performance. Fibers with higher aspect ratios can act as reinforcing elements that bridge across the binder matrix, improving tensile properties [36,37]. In contrast, shorter and thicker fibers increase the available interfacial area for binder adhesion, thereby enhancing cohesion but contributing less to load transfer [38]. Moreover, aspect ratio not only governs mechanical integrity but also affects the porosity and thermal insulation performance of fiber networks, as shown in simulation studies [39].

FTIR analysis confirmed cellulose as the dominant component, with characteristic O-H and C-H absorption bands, while some spectra also showed matches to blended textiles such as cotton-viscose (≈86%) and cotton-elastane (≈84%). These results demonstrate that the fibers originated from post-consumer waste rather than pure cotton (Table 2). Raman spectroscopy complemented these findings by identifying additional constituents, including polyester (≈69%), polypropylene (≈96%), and magnesium sulfate heptahydrate (≈66%). The detection of synthetic polymers and inorganic additives highlights the industrial processing history of the fibers and supports the conclusion that the recycled feedstock represents a complex mixture of natural, synthetic, and inorganic components (Table 2).

Table 2. Identified components of recycled cotton fibers by FTIR and Raman spectroscopy.

Method	Identified components	Notes / Match (%)
FTIR	Cellulose	Main component
	Cotton–viscose blend	86% match
	Cotton–elastane blend	84% match
Raman	Polyester	69% match
	Polypropylene	96% match
	Magnesium sulfate heptahydrate	66% match

Some spectra, however, indicated blended textiles, such as cotton-viscose or cotton-elastane, consistent with recent studies on mixed natural fibers [40,41]. Raman spectroscopy complemented these findings by identifying polyester, polypropylene, and magnesium sulfate heptahydrate, also reported in analyses of recycled cotton textiles [40]. The presence of hydroxyl-rich cellulose domains

 doi:10.20944/preprints202602.0834.v1

may enhance bonding with the PVAc-starch binder, whereas synthetic polymers provide less chemical interaction and may act as weak points. The detection of magnesium sulfate reflects the industrial finishing of cotton, supporting the conclusion that the fibers represent a heterogeneous mixture of natural, synthetic, and inorganic components typical of post-consumer waste.

To complement the spectroscopic analyses, EDS was performed to verify the elemental composition of the recycled fibers and to detect possible inorganic residues. The measurements confirmed carbon and oxygen as the dominant elements (≈34–68 wt.% C; 31–48 wt.% O), consistent with cellulose as the main component. Minor amounts of aluminum, sodium, and boron, as well as traces of rubidium, were also detected (Table 3). These findings support the FTIR and Raman results, indicating that the recycled fibers are chemically heterogeneous and contain residues of textile processing additives.

Table 3. Elemental composition (Mass%) of recycled cotton fiber samples measured by EDS.

Element	Sample 1	Sample 2	Sample 3
Boron (B)	2.96 ± 0.45	0.84 ± 0.26	–
Carbon (C)	33.77 ± 2.53	68.15 ± 3.94	46.71 ± 3.07
Oxygen (O)	43.19 ± 6.29	31.01 ± 6.76	47.79 ± 7.34
Sodium (Na)	5.08 ± 4.07	–	–
Aluminum (Al)	10.84 ± 9.34	–	5.50 ± 10.52
Rubidium (Rb)	4.17 ± 58.36	–	–

Such inorganic residues may slightly improve binder adhesion through increased surface activity but also contribute to chemical heterogeneity, potentially introducing weak points in the composite. Similar observations on residual elements affecting the interfacial properties of recycled fibers have been reported in recent studies [41,42].

3.2. Composite Thermal Insulation Board Morphology

The morphology of the composite boards is shown in Figure 4. At the macroscopic scale, the boards exhibited a rough surface with visible fiber fragments and inclusions, reflecting the heterogeneous nature of the recycled textile feedstock (Figure 4a). SEM analysis confirmed a porous network of entangled fibers interconnected by PVAc-starch binder domains (Figure 4b). The binder was observed in both continuous film and discrete granular forms, indicating its dual role in fiber bridging and pore filling.

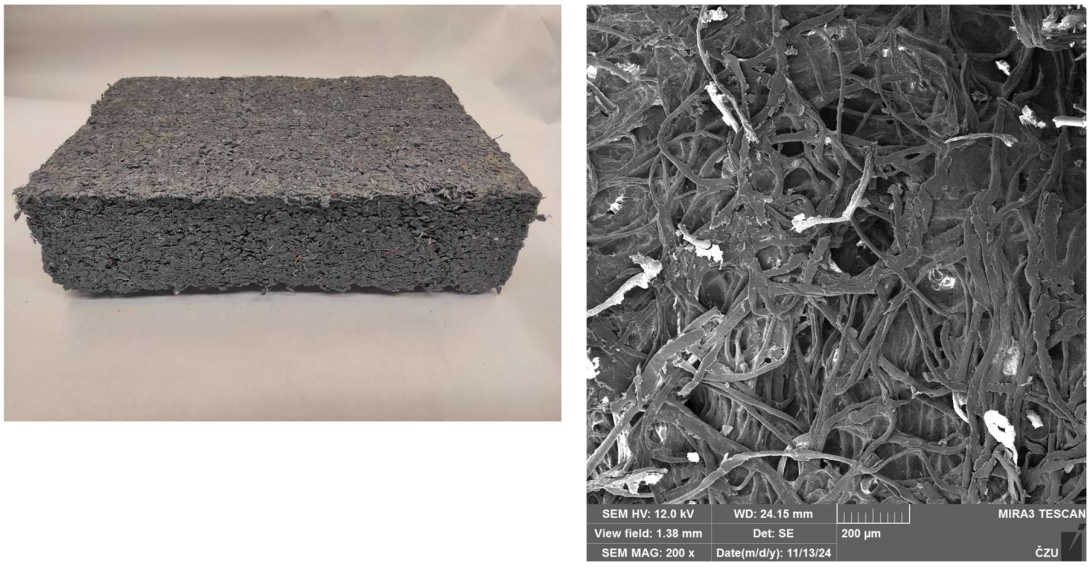

(**a**) (**b**)

Figure 4. Morphology of recycled cotton insulation boards: (**a**) macroscopic view and (**b**) SEM image.

 doi:10.20944/preprints202602.0834.v1

Such heterogeneity, typical of natural-fiber composites, is linked to strength variability [43,44], while the high porosity supports low thermal conductivity, as reported in porous fiber-based materials. At the same time, the open and interconnected pore structure may facilitate moisture uptake through capillary transport and sorption on hydrophilic fiber surface [45,46]. Excessive voids, however, may act as stress concentrators and limit structural reliability.

3.3. Bulk Density of Insulation Boards

For each formulation variant, multiple insulation boards were produced, and their bulk density was determined after conditioning. The measured bulk density values showed low variability within each density variant, with deviations not exceeding ± 5%.

The density values reported in tables and figures (300, 310, 320, 330, and 340 kg·m^{-3}) represent nominal target density classes used for sample designation and comparison. All reported material properties correspond to specimens whose measured bulk density fell within the defined tolerance range.

3.4. Thermal Parameters of the Thermal Insulation Board

Table 4 presents the mean values of thermal parameters (± standard deviation) obtained from nine measurements per density variant. Thermal conductivity showed a slight decreasing trend with higher density. In contrast, specific heat capacity varied across the tested range, reflecting differences in the heat storage capacity of the composites. Thermal diffusivity exhibited a non-monotonic dependence on density, resulting from the combined influence of thermal conductivity and volumetric heat capacity.

Table 4. Thermal Properties of Recycled Cotton Fiber Thermal Insulation Boards.

Density (kg·m^{-3})	Thermal Conductivity (W·m^{-1}·K^{-1})	Specific Heat Capacity (J·kg^{-1}·K^{-1})	Thermal Diffusivity (×10^{-6} m^2·s^{-1})
300	0.0738 ± 0.0003	1587 ± 93	0.155 ± 0.013
310	0.0730 ± 0.0006	1419 ± 59	0.166 ± 0.010
320	0.0724 ± 0.0003	1278 ± 85	0.177 ± 0.010
330	0.0710 ± 0.0006	916 ± 116	0.235 ± 0.044
340	0.0739 ± 0.0006	1294 ± 94	0.168 ± 0.011

In the present study, the thermal conductivity of recycled cotton fiber insulation boards ranged from 0.0710 to 0.0739 W·m^{-1}·K^{-1} at bulk densities of 300-340 kg·m^{-3}, which corresponds well with values reported for bio-based and recycled insulation materials. Comparable thermal conductivity values of 0.050-0.065 W·m^{-1}·K^{-1} were reported in recent study for natural fiber-reinforced insulation composites, emphasizing the influence of fiber structure and porosity on heat transfer [47]. Another study demonstrated that recycled textile-based insulation materials may reach λ values up to 0.140 W·m^{-1}·K^{-1}, depending on density and processing conditions, indicating that the results obtained in this study fall within the broader performance range of recycled fiber insulation systems [48]. In addition to thermal conductivity, the studied insulation boards exhibited relatively high specific heat capacity, which is characteristic of natural fiber-based materials and contributes to enhanced thermal inertia and delayed heat transfer through building envelopes [47,49].

One of the investigated variants exhibited noticeably deviating thermal properties compared to the trend of the remaining samples, which can be attributed to the inherent heterogeneity of recycled textile-based composites. The insulation boards were produced predominantly from recycled cotton fibers, while the binder system consisted of a PVA-starch mixture. In addition, fractions of synthetic fibers, originating from recycled textile waste, were present in the material, as confirmed by previous material analyses. Recent studies have demonstrated that even limited amounts of synthetic fibers, such as polyester or elastane, can locally affect heat transfer pathways due to their different intrinsic thermal properties compared to cotton fibers [50,51]. Furthermore, uneven distribution of polymer-based binders may partially fill pore spaces and increase fiber–fiber contact, leading to locally

 doi:10.20944/preprints202602.0834.v1

enhanced conductive heat transfer within fibrous insulation materials [52,53]. The observed deviation is most likely related to local material heterogeneity inherent in recycled textile composites.

3.5. Moisture-Related Behavior of the Thermal Insulation Board

Table 5 presents the mean values (± standard deviation) of water absorption (WA) and thickness swelling (TS) obtained from five specimens per density variant. Both parameters exhibited a clear decreasing trend with increasing board density, indicating lower moisture uptake and dimensional changes in denser composites. The observed variations among samples are attributed to the heterogeneous structure of the recycled fibers and the non-uniform distribution of the PVAc-starch binder.

Table 5. Short-term water absorption and dimensional stability of Recycled Cotton Fiber Thermal Insulation Boards.

Density (kg·m⁻³)	Height change (mm)	Depth change (mm)	Width change (mm)	Weight gain (g)	Water absorption WA (%)	Thickness swelling TS (%)
300	+1.8 ± 0.3	+4.4 ± 0.5	+1.6 ± 0.4	+258 ± 10	22.1 ± 0.9	5.6 ± 0.4
310	+1.5 ± 0.2	+4.3 ± 0.6	+1.3 ± 0.5	+240 ± 11	21.7 ± 1.0	5.1 ± 0.5
320	+1.2 ± 0.3	+3.9 ± 0.5	+1.1 ± 0.4	+230 ± 12	20.5 ± 0.8	4.8 ± 0.6
330	+1.0 ± 0.2	+3.5 ± 0.4	+1.0 ± 0.3	+220 ± 9	19.0 ± 0.7	4.3 ± 0.4
340	+0.9 ± 0.2	+3.2 ± 0.3	+0.8 ± 0.2	+210 ± 8	18.2 ± 0.6	3.9 ± 0.5

Water absorption and thickness swelling decreased with increasing board density, confirming that reduced porosity and higher binder content and improved binder distribution limit moisture penetration. In addition, denser boards contained a proportionally higher amount of the PVAc-starch adhesive, which filled voids more effectively and formed a partially continuous phase around fibers, thereby limiting capillary water uptake. Similar relationships between density and moisture uptake have been reported for natural-fiber composites, where micro voids and hydrophilic cellulose regions dominate water diffusion [44,45]. The obtained absorption levels (≈18–22%) are slightly higher than those reported for jute or flax composites, reflecting the inherently porous and hydrophilic nature of recycled cotton fibers. However, previous studies indicate that the application of hydrophobic surface treatments can effectively mitigate this effect and enhance dimensional stability under humid conditions [46].

3.6. Mechanical Properties of the Thermal Insulation Board

Figure 5 and Table 6 present the mean compressive strength values (± standard deviation) (σ_{10}) determined at 10% relative deformation for ten specimens per density variant, tested according to EN ISO 29469. The results show a consistent increase in compressive strength with increasing board density and with higher adhesive content, ranging from approximately 46 to 162 kPa.

Table 6. Compressive strength (mean values ± standard deviation) (σ_{10}) of thermal insulation boards at 10% deformation (EN ISO 29469, n = 10).

Density (kg·m⁻³)	Compressive strength σ_{10} (kPa)	Coefficient of variation (%)
300	45.6 ± 4.8	8.3
310	82.3 ± 6.1	7.4
320	98.7 ± 5.9	6.0
330	126.5 ± 7.2	5.7
340	162.4 ± 8.3	5.1

 doi:10.20944/preprints202602.0834.v1

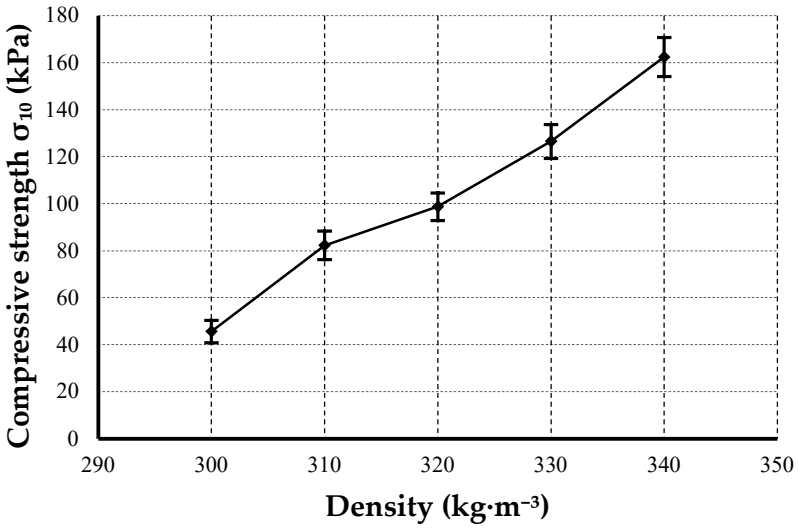

Figure 5. Variation of compressive strength (σ_{10}) with density for thermal insulation boards at 10 % deformation (EN ISO 29469 [33], n = 10). Vertical error bars represent standard deviations.

Compressive strength increased nearly linearly with density and higher adhesive content, confirming that higher fiber packing and binder content enhance stress transfer through the composite network. The improved binder fraction at greater compaction levels also contributed to stronger inter-fiber adhesion and more efficient load distribution. This trend aligns with findings reported for bio-based insulation and starch-reinforced composites, where densification reduces void content and enhances interfacial adhesion between fibers and the matrix [54,55]. The obtained strength levels (≈46-162 kPa) are consistent with previously published data for recycled or natural fiber–based panels [56]. The relatively low variation across samples demonstrates good fiber distribution and uniform binder dispersion. Similar improvements in compressive behavior due to higher starch or polymeric binder content were also observed in natural fiber-reinforced starch bio-composites [57,58].

Figure 6 and Table 7 show the internal bond strength (± standard deviation) (σ_{ib}) of thermal insulation boards, as determined according to EN ISO 29766 [34]. The mean tensile strength increased with board density from approximately 2 to 6 kPa.

Table 7. Internal bond strength (mean values ± standard deviation) (σ_{ib}) of thermal insulation boards at different densities determined according to EN ISO 29766 [34] (n = 10).

Density (kg·m⁻³)	Tensile strength σ_{ib} (kPa)	Coefficient of variation (%)
300	2.10 ± 0.25	11.9
310	2.40 ± 0.30	12.5
320	3.50 ± 0.40	11.4
330	6.10 ± 0.55	9.0
340	6.40 ± 0.60	9.4

 doi:10.20944/preprints202602.0834.v1

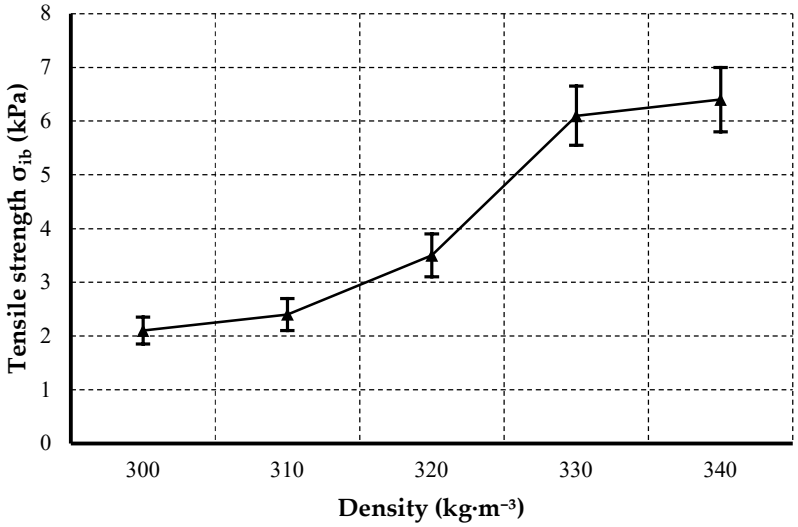

Figure 6. Variation of internal bond strength (σ_{ib}) with density for thermal insulation boards (EN ISO 29766 [34], n = 10). Vertical error bars represent standard deviations.

The internal bond strength increased from ~2.1 to ~6.4 kPa with increasing density and adhesive contend, indicating stronger inter-fiber cohesion and improved binder contact in denser composites. This relationship is in line with observations in wood-fiber insulation boards, where increased adhesive content or compaction boosted tensile strength perpendicular to the surface by 20-36 % [59]. The σ_{ib} values obtained here (≈2–6 kPa) are comparable to internal bond strengths reported in fiberboard panels made from recycled or natural fibers using bio-based binders [60]. Similar densification effects where increasing density or binder content enhances tensile integrity have been documented in other fiber–polymer systems, reflecting improved interfacial bonding and reduced void volume [61].

4. Conclusions

This study demonstrated that recycled cotton fibers can be effectively transformed into cohesive fiber-based insulation boards using a fully water-borne PVAc-starch binder system and a low-energy cold-pressing process. The resulting materials exhibited densities between 300 and 340 kg·m^{-3} and showed a balanced combination of thermal and mechanical performance, achieving thermal conductivity values of 0.0710-0.0739 W·m^{-1}·K^{-1}, compressive strengths of up to 160 kPa, and internal bond strengths exceeding 6 kPa. Increasing board density and binder content enhanced inter-fiber stress transfer and cohesion while preserving the lightweight and recyclable character of the fibrous structure. Although the materials remained moderately hydrophilic, improved binder distribution and reduced open porosity effectively mitigated moisture uptake. The demonstrated fabrication route, which is fully water-borne, formaldehyde-free, and conducted at room temperature, provides a low-energy and scalable pathway for the valorization of post-consumer cotton fibers into functional technical textile materials for insulation and building-related applications. Overall, the findings confirm that recycled cotton fiber-based boards represent a promising class of circular, low-impact materials combining satisfactory mechanical integrity with favorable thermal performance. Future work should focus on process optimization, moisture resistance enhancement, and scale-up considerations to support consistent industrial production.

Author Contributions: Conceptualization, P.Š. and T.Z.; methodology, P.Š. and T.Z.; software, T.Z and M.L.; validation, P.Š. and T.Z.; formal analysis, T.Z.; investigation, T.Z., P.Š., K.K., T.H., M.L., L.S., V.B.; resources, T.Z.; data curation, T.Z and P.Š..; writing—original draft preparation, T.Z.; writing—review and editing, T.Z.,

 doi:10.20944/preprints202602.0834.v1

P.Š.,V.B., A.S.; visualization, T.Z.; supervision, P.Š., V.B., A.S.; project administration, T.Z.; funding acquisition, T.Z. All authors have read and agreed to the published version of the manuscript.

Funding: The research was carried out as part of the project entitled "Development and analyses of thermal insulation materials based on cellulose fibers", no. A_09_23 of the program of the Internal Grant Agency of the Faculty of Forestry and Wood, Czech University of Life Sciences in Prague.

Institutional Review Board Statement: Not applicable.

Data Availability Statement: Data is available on request due to ethical restrictions. The data presented in this study are available on request from the corresponding author. The data is not publicly available due to unfinished research.

Acknowledgments: Thanks to the support of the Department of Wood Processing and Biomaterials at the Faculty of Forestry and Wood Technology.

Conflicts of Interest: The Authors declare no conflict of interest.

Abbreviations

A	Loaded cross-sectional area of specimen (mm^2)
a	Thermal diffusivity ($m^2 \cdot s^{-1}$)
c	Specific heat capacity ($J \cdot kg^{-1} \cdot K^{-1}$)
d	Specimen thickness (m)
F	Load (N)
λ	Thermal conductivity ($W \cdot m^{-1} \cdot K^{-1}$)
L	Specimen length (mm)
m_0	Mass of specimen before immersion (g)
m_1	Mass of specimen after immersion (g)
ρ	Density ($kg \cdot m^{-3}$)
$\rho \cdot c$	the volumetric heat capacity ($J \cdot m^{-3} \cdot K^{-1}$)
σ_{10}	Compressive strength at 10% deformation (kPa)
σ_{ib}	Internal bond strength (tensile strength perpendicular to board plane) (kPa)
t_0	Initial specimen thickness before immersion (mm)
t_1	Specimen thickness after immersion (mm)
T	Specimen thickness (mm)
TS	Thickness swelling (dimensional change after immersion) (%)
V	Specimen volume (m^3)
W	Specimen width (mm)
WA	Water absorption (mass increase after immersion) (%)

References

1. Hu, S.; Cabeza, L.F.; Yan, D. Review and Estimation of Global Halocarbon Emissions in the Buildings Sector. *Energy and Buildings* **2020**, *225*, 110311, doi:10.1016/j.enbuild.2020.110311.
2. Islam, S.; Bhat, G. Environmentally-Friendly Thermal and Acoustic Insulation Materials from Recycled Textiles. *Journal of Environmental Management* **2019**, *251*, 109536, doi:10.1016/j.jenvman.2019.109536.
3. Angelotti, A.; Alongi, A.; Augello, A.; Dama, A.; De Antonellis, S.; Ravidà, A.; Zinzi, M.; De Angelis, E. Thermal Conductivity Assessment of Cotton Fibers from Apparel Recycling for Building Insulation. *Energy and Buildings* **2024**, *324*, 114866, doi:10.1016/j.enbuild.2024.114866.
4. Saran, C.S.; Satapathy, A. Epoxy-hemp and Epoxy-flax Composites Filled with Glass Dust for Enhanced Thermal Insulation: An Analytical and Experimental Study. *Polymer Composites* **2024**, *45*, 5244–5255, doi:10.1002/pc.28123.

 doi:10.20944/preprints202602.0834.v1

5. Guo, L.; Wang, F.; Li, H. Preparation and Characterization of Cellulose Nanofiber/Melamine–Urea–Formaldehyde Composite Aerogels for Thermal Insulation Applications. *Polymer Composites* **2022**, *43*, 7882–7892, doi:10.1002/pc.26910.
6. Reza, M.M.; Begum, H.A.; Uddin, A.J. Potentiality of Sustainable Corn Starch-Based Biocomposites Reinforced with Cotton Filter Waste of Spinning Mill. *Heliyon* **2023**, *9*, e15697, doi:10.1016/j.heliyon.2023.e15697.
7. Wang, X.; Liu, W.; Zeng, L.; Zhang, L.; Bai, C.; Shen, J.; Zheng, T.; Sun, B.; Qiao, Y. Lightweight, Hydrostatic Pressure-resistance, Thermal Insulating Epoxy Syntactic Foam with a Multiscale Ternary Structure for Marine Engineering Application. *Polymer Composites* **2024**, *45*, 9703–9712, doi:10.1002/pc.28431.
8. Feng, J.; Li, N.; Wang, B.; Cheng, S.; Bao, Q.; Wang, H.; Jian, X. Thermal Insulation and Mechanical Properties of Carbon Fiber-reinforced Thermoplastic Polyphthalazine Ether Sulfone Ketone Composites Reinforced by Hollow Glass Beads. *Polymer Composites* **2023**, *44*, 7941–7952, doi:10.1002/pc.27677.
9. Bello, K.O.; Yan, N. Mechanical and Insulation Performance of Rigid Polyurethane Foam Reinforced with Lignin-Containing Nanocellulose Fibrils. *Polymers* **2024**, *16*, 2119, doi:10.3390/polym16152119.
10. Cárdenas-Oscanoa, A.J.; Tene Tayo, J.L.; Huang, C.; Huang, C.; Euring, M. Discovering Natural Fiber-Insulation Boards and Natural Adhesives, Focused on a Polylactic Acid (PLA) Application – a Review. *Journal of Natural Fibers* **2024**, *21*, 2343371, doi:10.1080/15440478.2024.2343371.
11. Directive (EU) 2024/1275 of the European Parliament and of the Council of 24 April 2024 on the Energy Performance of Buildings (Recast) (Text with EEA Relevance).
12. Islam, S.; Bhat, G.; Mani, S. Life Cycle Assessment of Thermal Insulation Materials Produced from Waste Textiles. *J Mater Cycles Waste Manag* **2024**, *26*, 1071–1085, doi:10.1007/s10163-023-01882-7.
13. Rebolledo, P.; Cloutier, A.; Yemele, M.-C. Effect of Density and Fiber Size on Porosity and Thermal Conductivity of Fiberboard Mats. *Fibers* **2018**, *6*, 81, doi:10.3390/fib6040081.
14. Andrä, H.; Dobrovolskij, D.; Engelhardt, M.; Godehardt, M.; Makas, M.; Mercier, C.; Rief, S.; Schladitz, K.; Staub, S.; Trawka, K.; et al. Image-Based Microstructural Simulation of Thermal Conductivity for Highly Porous Wood Fiber Insulation Boards: 3D Imaging, Microstructure Modeling, and Numerical Simulations for Insight into Structure–Property Relation. *Wood Sci Technol* **2023**, *57*, 5–31, doi:10.1007/s00226-022-01434-6.
15. Carvajal, S.A.; Paulien, L.; Elniski, A.; Daryabeigi, K.; Berg, M.J. Analytical Models of Radiative Transfer in Fibrous Insulation under Collimated Irradiation. *International Journal of Heat and Mass Transfer* **2025**, *244*, 126961, doi:10.1016/j.ijheatmasstransfer.2025.126961.
16. Liu, H.; Zhao, X. Thermal Conductivity Analysis of High Porosity Structures with Open and Closed Pores. *International Journal of Heat and Mass Transfer* **2022**, *183*, 122089, doi:10.1016/j.ijheatmasstransfer.2021.122089.
17. Ruan, K.; Shi, X.; Guo, Y.; Gu, J. Interfacial Thermal Resistance in Thermally Conductive Polymer Composites: A Review. *Composites Communications* **2020**, *22*, 100518, doi:10.1016/j.coco.2020.100518.
18. Hsissou, R.; Seghiri, R.; Benzekri, Z.; Hilali, M.; Rafik, M.; Elharfi, A. Polymer Composite Materials: A Comprehensive Review. *Composite Structures* **2021**, *262*, 113640, doi:10.1016/j.compstruct.2021.113640.
19. Zha, J.-W.; Wang, F.; Wan, B. Polymer Composites with High Thermal Conductivity: Theory, Simulation, Structure and Interfacial Regulation. *Progress in Materials Science* **2025**, *148*, 101362, doi:10.1016/j.pmatsci.2024.101362.
20. Barboutis, I.; Kamperidou, V. Shear Strength of Beech Wood Joints Bonded with Commercially Produced PVAc D3 Adhesives. *International Journal of Adhesion and Adhesives* **2021**, *105*, 102774, doi:10.1016/j.ijadhadh.2020.102774.
21. Gadhave, R.V.I.; Dhawale, P.V. State of Research and Trends in the Development of Polyvinyl Acetate-Based Wood Adhesive. *OJPChem* **2022**, *12*, 13–42, doi:10.4236/ojpchem.2022.121002.
22. Gadhave, R.V. Water-Resistant Wood Adhesive without Plasticizers: Synthesis and Characterization. *J Indian Acad Wood Sci* **2024**, *21*, 135–146, doi:10.1007/s13196-024-00332-7.
23. Yin, H.; Zheng, P.; Zhang, E.; Rao, J.; Lin, Q.; Fan, M.; Zhu, Z.; Zeng, Q.; Chen, N. Improved Wet Shear Strength in Eco-Friendly Starch-Cellulosic Adhesives for Woody Composites. *Carbohydrate Polymers* **2020**, *250*, 116884, doi:10.1016/j.carbpol.2020.116884.

 doi:10.20944/preprints202602.0834.v1

24. Chen, Y.; Rao, Y.; Liu, P.; Han, Z.; Xie, F. Facile Fabrication of a Starch-Based Wood Adhesive Showcasing Water Resistance, Flame Retardancy, and Antibacterial Properties via a Dual Crosslinking Strategy. *International Journal of Biological Macromolecules* **2024**, *282*, 137180, doi:10.1016/j.ijbiomac.2024.137180.
25. Vineeth, S.K.; Gadhave, R.V. Corn Starch Blended Polyvinyl Alcohol Adhesive Chemically Modified by Crosslinking and Its Applicability as Polyvinyl Acetate Wood Adhesive. *Polym. Bull.* **2024**, *81*, 811–825, doi:10.1007/s00289-023-04746-0.
26. Ghasemirad, S.; Ahmadi-Dehnoei, A.; Shahabi-Sirmandi, P. Improvement of Shear Strength of Starch-Based Wood Adhesives Using Polysilsesquioxane/Polyvinyl Acetate Hybrid Nanoparticles. *International Journal of Biological Macromolecules* **2025**, *304*, 140891, doi:10.1016/j.ijbiomac.2025.140891.
27. European Organisation for Technical Assessment (EOTA) *AED 0404138-01-1201: IN-SITU FORMED LOOSE FILL THERMAL AND/OR ACOUSTIC INSULATION PRODUCTS MADE OF VEGETABLE FIBRES*; EOTA, Brussels, 2018;
28. Mawardi, I.; Aprilia, S.; Faisal, M.; Rizal, S. Characterization of Thermal Bio-Insulation Materials Based on Oil Palm Wood: The Effect of Hybridization and Particle Size. *Polymers* **2021**, *13*, 3287, doi:10.3390/polym13193287.
29. Raja, P.; Murugan, V.; Ravichandran, S.; Behera, L.; Mensah, R.A.; Mani, S.; Kasi, A.; Balasubramanian, K.B.N.; Sas, G.; Vahabi, H.; et al. A Review of Sustainable Bio-Based Insulation Materials for Energy-Efficient Buildings. *Macro Materials & Eng* **2023**, *308*, 2300086, doi:10.1002/mame.202300086.
30. Tupciauskas, R.; Berzins, A.; Pavlovics, G.; Bikovens, O.; Filipova, I.; Andze, L.; Andzs, M. Optimization of Thermal Conductivity vs. Bulk Density of Steam-Exploded Loose-Fill Annual Lignocellulosics. *Materials* **2023**, *16*, 3654, doi:10.3390/ma16103654.
31. International Organization for Standardization. *Thermal Insulation — Determination of Steady-State Thermal Resistance and Related Properties — Heat Flow Meter Apparatus*; ISO 8301:1991; Geneva, Switzerland, **1991**.
32. International Organization for Standardization. *Thermal Insulating Products for Building Applications — Determination of Short-Term Water Absorption by Partial Immersion*; ISO 29767:2019; Geneva, Switzerland, **2019**.
33. International Organization for Standardization. *Thermal Insulating Products for Building Applications — Determination of Compression Behaviour*; ISO 29469:2022; Geneva, Switzerland, **2022**.
34. International Organization for Standardization. *Thermal Insulating Products for Building Applications — Determination of Tensile Strength Parallel to Faces*; ISO 29766:2022; Geneva, Switzerland, **2022**.
35. Kärkkäinen, E.; Kamppuri, T.; Heikinheimo, L.; Silva, C.J.; Gomes, J.M. Characterisation of Fibre Mechanical Recycled Cotton Denim Fibres and the Effects of Their Properties on Yarns and Knits. *Recycling* **2025**, *10*, 177, doi:10.3390/recycling10050177.
36. Pandurangan, T.E.; Venkateshwaran, N.; Rajini, N.; Sivaranjana, P.; Alavudeen, A.; Ismail, S.O. Fiber Aspect Ratio and Its Effects on Mechanical Properties of Pineapple Leaf Fiber Composites. In *Biocomposites - Bio-Based Fibers and Polymers from Renewable Resources*; Elsevier, 2024; pp. 235–245 ISBN 978-0-323-97282-6.
37. Shams, A.T.; Papon, E.A.; Haque, A. The Effects of Fiber Concentration, Orientation, and Aspect Ratio on the Frontal Polymerization of Short Carbon-Fiber-Reinforced Composites: A Numerical Study. *J. Compos. Sci.* **2025**, *9*, 307, doi:10.3390/jcs9060307.
38. Azevedo, T.; Silva, A.C.; Machado, G.; Chaves, D.; Ribeiro, A.I.; Fangueiro, R.; Ferreira, D.P. Reinforcing Cotton Recycled Fibers for the Production of High-Quality Textile Structures. *Polymers* **2025**, *17*, 1392, doi:10.3390/polym17101392.
39. Sahoo, B.; Nanda, B.P. Effect of Fiber Aspect Ratio and Orientation on the Thermal Insulation Property of Short Palm Leaf Fiber Reinforced Epoxy Composite. *Next Materials* **2025**, *9*, 101092, doi:10.1016/j.nxmate.2025.101092.
40. Puchowicz, D.; Cieslak, M. Raman Spectroscopy in the Analysis of Textile Structures. In *Recent Developments in Atomic Force Microscopy and Raman Spectroscopy for Materials Characterization*; Shakher Pathak, C., Kumar, S., Eds.; IntechOpen, 2022 ISBN 978-1-83968-229-2.
41. Neto, J.S.S.; De Queiroz, H.F.M.; Aguiar, R.A.A.; Banea, M.D. A Review on the Thermal Characterisation of Natural and Hybrid Fiber Composites. *Polymers* **2021**, *13*, 4425, doi:10.3390/polym13244425.

 doi:10.20944/preprints202602.0834.v1

42. Patel, R.V.; Yadav, A.; Winczek, J. Physical, Mechanical, and Thermal Properties of Natural Fiber-Reinforced Epoxy Composites for Construction and Automotive Applications. *Applied Sciences* **2023**, *13*, 5126, doi:10.3390/app13085126.
43. Tasgin, Y.; Demircan, G.; Kandemir, S.; Acikgoz, A. Mechanical, Wear and Thermal Properties of Natural Fiber-Reinforced Epoxy Composite: Cotton, Sisal, Coir and Wool Fibers. *J Mater Sci* **2024**, *59*, 10844–10857, doi:10.1007/s10853-024-09810-2.
44. Mohammed, M.; Jawad, A.J.M.; Mohammed, A.M.; Oleiwi, J.K.; Adam, T.; Osman, A.F.; Dahham, O.S.; Betar, B.O.; Gopinath, S.C.B.; Jaafar, M. Challenges and Advancement in Water Absorption of Natural Fiber-Reinforced Polymer Composites. *Polymer Testing* **2023**, *124*, 108083, doi:10.1016/j.polymertesting.2023.108083.
45. Pavlovic, A.; Valzania, L.; Minak, G. Effects of Moisture Absorption on the Mechanical and Fatigue Properties of Natural Fiber Composites: A Review. *Polymers* **2025**, *17*, 1996, doi:10.3390/polym17141996.
46. Wang, Q.; Chen, T.; Wang, X.; Zheng, Y.; Zheng, J.; Song, G.; Liu, S. Recent Progress on Moisture Absorption Aging of Plant Fiber Reinforced Polymer Composites. *Polymers* **2023**, *15*, 4121, doi:10.3390/polym15204121.
47. Ouda, M.; Abu Sanad, A.A.; Abdelaal, A.; Krishna, A.; Kandah, M.; Kurdi, J. A Comprehensive Review of Sustainable Thermal and Acoustic Insulation Materials from Various Waste Sources. *Buildings* **2025**, *15*, 2876, doi:10.3390/buildings15162876.
48. Majumder, A.; Canale, L.; Mastino, C.C.; Pacitto, A.; Frattolillo, A.; Dell'Isola, M. Thermal Characterization of Recycled Materials for Building Insulation. *Energies* **2021**, *14*, 3564, doi:10.3390/en14123564.
49. Vėjelis, S.; Vaitkus, S.; Skulskis, V.; Kremensas, A.; Kairytė, A. Performance Evaluation of Thermal Insulation Materials from Sheep's Wool and Hemp Fibres. *Materials* **2024**, *17*, 3339, doi:10.3390/ma17133339.
50. Dama, A.; Khalfallaand, E.A.M.; Alongi, A.; Angelotti, A. Thermal Performance Characterization of Recycled Textile-Based Materials for Building Insulation. In *The 1st International Conference on Net-Zero Built Environment*; Kioumarsi, M., Shafei, B., Eds.; Lecture Notes in Civil Engineering; Springer Nature Switzerland: Cham, 2025; Vol. 237, pp. 449–460 ISBN 978-3-031-69625-1.
51. Dama, A.; Khoshtinat, S.; Alongi, A.; Marano, C.; Angelotti, A. Hygro-Thermal and Acoustic Performances of Recycled Textile-Based Materials for Building Applications. *Developments in the Built Environment* **2025**, *22*, 100657, doi:10.1016/j.dibe.2025.100657.
52. Cárdenas-Oscanoa, A.J.; Tene Tayo, L.; Huang, C.; Huang, C.; Shivappa Nayaka, D.; Euring, M. Wood-Fiber Insulation Boards Produced with Polylactic Acid as a Binder by Hot Press and Hot Air. *Eur. J. Wood Prod.* **2025**, *83*, 23, doi:10.1007/s00107-024-02153-4.
53. Mouguen, F.; Charai, M.; Oubaha, S.; Mghazli, M.O.; Mezrhab, A.; Taha, Y.; Benzaazoua, M. Synergistic Optimization of Plant-Based Natural Insulation Materials with Starch and Waste-Expanded Polystyrene Composite Binders: Advancing Thermo-Acoustic Efficiency for Sustainable Building Envelopes. *Energy and Buildings* **2025**, *341*, 115834, doi:10.1016/j.enbuild.2025.115834.
54. Mundhe, A.; Kandasubramanian, B. Advancements in Natural Fiber Composites: Innovative Chemical Surface Treatments, Characterizaton Techniques, Environmental Sustainability, and Wide-Ranging Applications. *Hybrid Advances* **2024**, *7*, 100282, doi:10.1016/j.hybadv.2024.100282.
55. McKay, I.; Vargas, J.; Yang, L.; Felfel, R.M. A Review of Natural Fibres and Biopolymer Composites: Progress, Limitations, and Enhancement Strategies. *Materials* **2024**, *17*, 4878, doi:10.3390/ma17194878.
56. Schritt, H.; Pleissner, D. Recycling of Organic Residues to Produce Insulation Composites: A Review. *Cleaner Waste Systems* **2022**, *3*, 100023, doi:10.1016/j.clwas.2022.100023.
57. Kibet, T.; Githinji, D.N.; Nziu, P. Natural Fibre–Reinforced Starch Biocomposites and Their Effects on the Material Mechanical Properties: A Review. *Advances in Materials Science and Engineering* **2025**, *2025*, 9905014, doi:10.1155/amse/9905014.
58. Khoaele, K.K.; Mphahlele, I.J.; Gbadeyan, O.J.; Sithole, B.; Chunilall, V. Current Approaches on Natural Fiber Reinforcement Surface Treatment for Construction Material Application. *International Journal of Polymer Science* **2024**, *2024*, 1387468, doi:10.1155/2024/1387468.

 doi:10.20944/preprints202602.0834.v1

59. Segovia, F.; Blanchet, P.; Auclair, N.; Essoua Essoua, G. Thermo-Mechanical Properties of a Wood Fiber Insulation Board Using a Bio-Based Adhesive as a Binder. *Buildings* **2020**, *10*, 152, doi:10.3390/buildings10090152.
60. Antov, P.; Krišťák, L.; Réh, R.; Savov, V.; Papadopoulos, A.N. Eco-Friendly Fiberboard Panels from Recycled Fibers Bonded with Calcium Lignosulfonate. *Polymers* **2021**, *13*, 639, doi:10.3390/polym13040639.
61. Ahmad, W.; McCormack, S.J.; Byrne, A. Biocomposites for Sustainable Construction: A Review of Material Properties, Applications, Research Gaps, and Contribution to Circular Economy. *Journal of Building Engineering* **2025**, *105*, 112525, doi:10.1016/j.jobe.2025.112525.